Low pressure plasma-jet systems and their application for deposition of ceramic thin films

Z. HUBIČKA[a], M. CHICHINA[a,b], A. DEYNEKA[a], P. KUDRNA[a,b], J. OLEJNÍČEK[a], H. ŠÍCHOVÁ[b], M. ŠÍCHA[a,b], L. JASTRABÍK[a], P. VIROSTKO[a,b], P. ADÁMEK[c], M. TICHÝ[b]
[a]*Institute of Physics, Academy of Sciences of the Czech Rep., Na Slovance 2, 182 21 Prague 8, Czech Republic*
[b]*Charles University in Prague, Fac. of Math. and Physics, V Holešovičkách 2, 180 00 Prague 8, Czech Republic*
[c]*University of South Bohemia, Fac. of Education, Jeronýmova 10, 371 15 České Budějovice, Czech Republic*

We applied the single and the double hollow cathode plasma jet systems for deposition of $Ba_xSr_{1-x}TiO_3$ (BSTO) thin films on Si and on multi-layer $Si/SiO_2/TiO_2/Pt$ substrates. Two ceramic inserts in a single nozzle or two separate nozzles made of $BaTiO_3$ (BTO) and $SrTiO_3$ (STO) ceramics were reactively sputtered in the RF modulated plasma jet. The substrate was simultaneously heated on approximately 500 °C. Plasma parameters during the deposition process were determined by time-resolved measurements over the working (active pulse) and the idle part of the period. Electron density and electron effective temperature at the substrate position were determined by Langmuir probe technique, temperature of neutral particles and ratio of sputtered atoms (especially Ba and Sr) were estimated by optical emission spectroscopy. Elemental composition of the deposited films was estimated by electron microprobe analysis. Measured electron concentration in the substrate position reached value 2×10^{16} m^{-3} during the active part of the duty cycle and resulting effective electron temperature was approximately 5 eV. Temperature of neutral particles measured by means of rotational temperature of OH radicals was lower than 500 K and high correlation between ratio of spectral intensity of Ba and Sr lines and ratio of Ba and Sr atoms in BSTO thin film was observed. Knowledge of this correlation was used for deposition of compositional gradient BSTO thin films. XRD diffraction confirmed presence of BSTO and STO perovskite phase in the films.

(Received November 2, 2006; accepted February 28, 2007)

Keywords: Plasma jet, Langmuir probe, STO and BSTO layers, Ceramic thin films

1. Introduction

The low pressure RF plasma jet sputtering system was already used for many PVD thin films depositions, e.g. TiN [1], TiO_2 [2], Cu_3N [3], CN_x [4] and $LiCoO_x$ [5]. In these applications, usually a metallic or single component hollow cathode was reactively sputtered in a suitable working gas.

Ferroelectric thin films like barium titanate $BaTiO_3$ (BTO) or barium strontium titanate $Ba_xSr_{1-x}TiO_3$ (BSTO) that combine the merits of the high permittivity of $BaTiO_3$ with the structural stability of $SrTiO_3$ (STO) represent a promising material for many electronic applications. Due to their dielectric properties it is possible to use them in dynamic random access memories (DRAM), tunable microwave systems, electro-optic switches and many others. BSTO thin films are usually prepared by CVD, MOCVD [6], sol-gel and magnetron sputtering [7]. An alternative approach will be presented in this paper where either the single RF hollow cathode provided by two inserts made of $SrTiO_3$ (STO) and $BaTiO_3$ (BTO) ceramics or two hollow cathodes with inserts from both materials respectively were reactively sputtered in Ar and O_2 gas mixture in order to form $SrTiO_3$, $Ba_xSr_{1-x}TiO_3$ films on Si and multi-layer $Si/SiO_2/TiO_2/Pt$ substrates.

The pulse modulated plasma sources are nowadays often used for plasma-aided deposition of layers from technologically important materials. The pulse modulation adds namely another “control dimension” to the plasma-chemical process, which resides in the possibility to change the duty cycle. That enables adjusting high plasma density during the active pulse while keeping low the *average* power deposited to the plasma, to the target and to the substrate. Especially for deposition of ceramic layers when it is difficult to cool down the target because of its low thermal conductivity, the impulse modulation of the plasma source is indispensable.

2. Experimental system

Experimental setup with *single* hollow cathode plasma jet can be seen in Fig. 1. The discharge was operated in a reactor chamber, which was continuously pumped by combination of Roots and rotary vane pumps. Working pressure was held at $p = 6$ Pa during all measurements with single-jet system. The cylindrical nozzle acts as RF hollow cathode, which is reactively sputtered. RF power has to be used for plasma excitation because both the used nozzle materials are dielectrics. The internal diameter of the nozzle is 3 mm. Its total length is 30 mm. The nozzle was composed of two parts as it can be seen in Fig. 1. In order to deposit $SrTiO_3$ thin films the nozzle was homogeneous: both parts made of pure $SrTiO_3$ ceramic. In order to deposit $Ba_xSr_{1-x}TiO_3$ thin films one part of the nozzle was made of $SrTiO_3$ and the other part of $BaTiO_3$. Since it was known that STO ceramics has

lower sputtering yield than BTO ceramics the STO part was closer to the nozzle outlet where the hollow cathode plasma had higher density and was longer than BTO part. The length of STO part was 25 mm and BTO part 5 mm. The substrate was placed perpendicularly to the plasma jet axis at the distance 20 mm from the nozzle outlet.

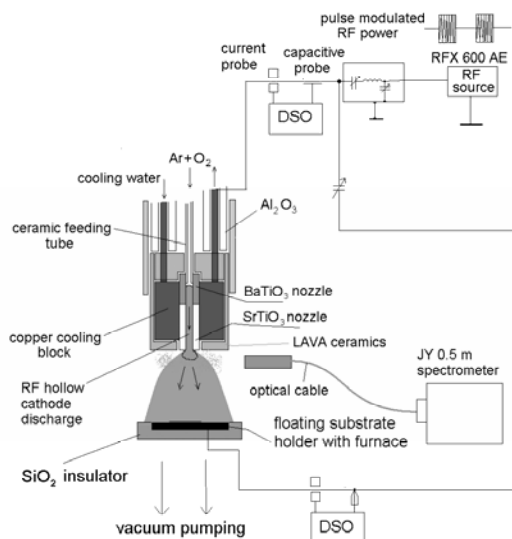

Fig. 1. Experimental set up for the single-nozzle plasma jet deposition of STO and BSTO thin films.

As an RF source capable of being pulse modulated the Advanced Energy RFX600 was used. The applied power averaged over the modulation cycle did not exceed 500 W in all experiments. Length of the modulation cycle T_M was variable from 1 ms to 10 ms (repetition frequency 100 Hz – 1 kHz), and the length of the active part of the cycle T_A from 50 ms up to 1 ms. In the active part of the modulation cycle an intensive RF hollow cathode discharge was generated inside the nozzle, on the background of a primary capacitive RF plasma excited in the volume of the reactor [8]. Incoming working gas, which was fed through the nozzle, forced the hollow cathode discharge out of the nozzle into the reactor chamber. Mixture of argon and molecular oxygen was used as working gas.

The low-pressure *double* hollow cathode plasma jet system for BSTO thin films deposition can be seen in Fig. 2. The reactor chamber was continuously pumped by combination of Roots and rotary vane pump during the deposition. The internal diameter of the nozzles was 3 mm and the length was 30 mm. These nozzles work as RF hollow cathodes that are sputtered in Ar and O_2 atmosphere at working pressure $p = 5$ Pa. The first nozzle was made of pure BTO ceramics, and the second one was made of STO ceramics. The angle between both nozzles was 90° and the angle between nozzle and substrate was 45°. (To enhance the clarity these angles are somewhat distorted in Fig. 2.) Flow rates of Ar and O_2 in both nozzles were Q_{Ar} =60 sccm and Q_{O2} = 30 sccm. The substrate was placed 30 mm from both the nozzle outlets. The temperature of the substrate was held on 500 °C in the single nozzle and on 450 °C in the double nozzle experiments.

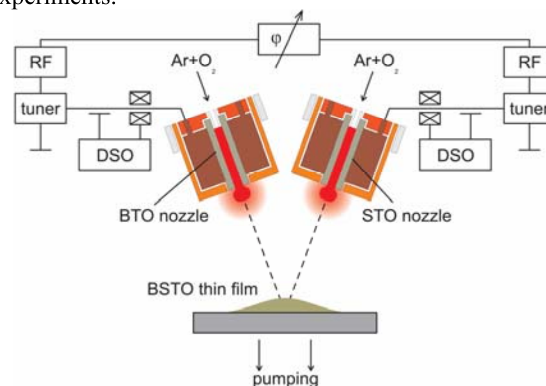

Fig. 2. Double hollow cathode plasma jet system for BSTO thin film deposition.

STO and BSTO thin films were deposited simultaneously on Si wafers and on the Pt top layer of multi-layer $Si/SiO_2/TiO_2/Pt$ substrate. Analysis of films structure was performed by XRD diffraction in Bragg-Brentano and GI geometry using CuK_α radiation. Chemical composition of deposited films was measured by electron microprobe JXA 733 by JEOL. For all the discussed STO and BSTO samples, pulse modulated mode was used for the plasma jet excitation. In single nozzle experiments RF power P_{RF} = 200 – 400 W was applied on the hollow nozzle electrode in the active part of the modulation cycle, no power in the idle part of the cycle. The length of the active part was T_w = 1.2 ms and of the idle part T_0 = 4 ms (repetition frequency 192 Hz) in single nozzle experiments. In double nozzle experiments the absorbed RF power during active part of the modulation cycle was approximately 300 W. The modulation frequency used in both RF generators was f = 535 Hz (period approximately 1.87 ms). The active part of the period was 770 µs, the idle part was 1100 µs for both the STO and BTO nozzles. To avoid beating of frequencies from both RF generators (we did not have the possibility of synchronizing them) the discharges in particular nozzles were excited sequentially. In other words the falling edge of the active pulse of one generator triggered the rising edge of the active pulse of the other generator. In case of deposition of compositional gradient thin films with changeable value of parameter x in stoichiometric formula $Ba_xSr_{1-x}TiO_3$ the ratio of active and idle parts of pulse for BTO and STO nozzles was changed but the frequency remained stable. Change of the duty cycle produced change in average power and also sputtering rate. Current and voltage probes calibrated for RF amplitude response, and phase shift up to 100 MHz in combination with digital oscillograph Infinium Agilent 600 MHz 4 GS/s were capable of measuring the RF current and RF voltage waveforms on the nozzle(s). The RF power absorbed in the discharge and the discharge impedance was calculated from these measurements. The negative DC self-bias was set always on U_{DC} = 50 V relative to grounded reactor.

Optical emission spectroscopy was used for monitoring of sputtered species contained in the plasma jet channel. For this purpose we exploited the Jobin Yvon Triax 550 spectrometer provided by CCD detector and optical cable.

The electron density and the mean electron energy (effective electron temperature) in the plasma channel were measured by time resolved Langmuir probe technique at the same conditions as used for deposition experiments. The probe was positioned on the cylindrical axis of the plasma jet at the distance l_S = 38 mm from the nozzle end in the single jet case and at the distance l_S = 30 mm from both nozzle outlets in the double jet case. The substrate holder was not present in the reactor chamber during Langmuir probe measurements.

Platinum cylindrical Langmuir probe with diameter d_p = 20 μm and length l_p = 2 mm was applied. The grounded metallic reactor worked as a voltage reference electrode for the Langmuir probe. High impedance filters and a metallic cylindrical compensation electrode connected with the probe through a capacitor, see e.g. [9], minimized the effect of RF oscillations on probe characteristic.

Synchronization unit implemented in the probe system allowed measuring all points of single characteristic at a defined time *t* from the beginning of modulation cycle.

The probe surface was cleaned from deposited non-conducting film by applying high negative voltage on the probe between probe characteristic measurements. This caused ion bombardment and consequently sputtering of the material deposited on the probe surface.

3. Results and discussion

3.1 Results of Langmuir probe measurements

The relevant results obtained in experiments with the single nozzle system were very similar to those obtained in experiments with the double nozzle one. Since the double nozzle system offers advantages in comparison to the single nozzle one from the point of view of deposition technology we present here only the experimental results gained with the double nozzle system. The time resolved probe measurements in the double nozzle system were performed when only one nozzle was operational (BTO nozzle was off). From the measured probe characteristic we determined the electron density from the electron current at the plasma potential. That requires assumption of the Maxwellian electron energy distribution function (EEDF). Since the measured EEDF was Maxwellian neither in the active nor in the afterglow phase of the modulation cycle we estimated the electron density also from the integral of the EEDF. The EEDF was calculated from the second derivative of the electron probe current according to the Druyvesteyn formula [10]. In our calculations we assumed the second derivative of the probe positive ion current to be negligible and hence the EEDF was calculated from the second derivative of the total probe current. Plasma potential was determined as the probe voltage at which the zero crossing of the second derivative of the probe current occurs. By using the estimated EEDF there was also possible to calculate the electron mean energy and, consequently, the effective electron temperature. The applied techniques of probe characteristic interpretation were the standard ones described e.g. in [11]. The measured courses of the electron density and of the electron mean energy over the modulation cycle are depicted in Fig. 3 and Fig. 4 respectively.

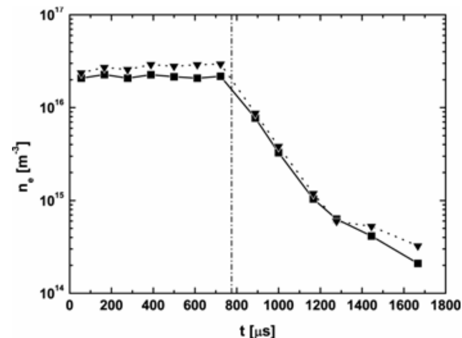

Fig. 3. *Time evolution of the electron density. Black squares represent the electron density computed from the integral of the EEDF. Black triangles represent the electron density computed from the plasma potential.*

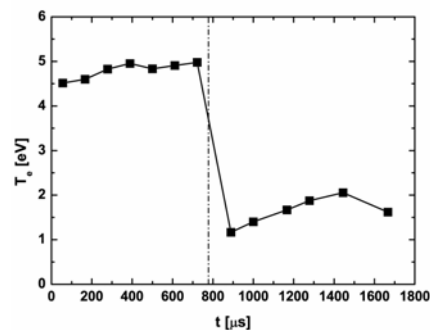

Fig. 4. Time evolution of the effective electron temperature T_e. A vertical dash-dot line indicates the end of active part of the pulse.

The decay of the electron density with afterglow time in Fig. 3 is approximately exponential. That can be explained by the diffusion as the major decay process. Indeed, the atomic argon ions do not recombine fast since the most probable recombination mechanism at the used pressure is the radiative recombination with very slow rate. In case that there were large density of O_2^+ ions the process of their fast recombination would overwhelm the diffusion and the decay line of the electron density in Fig. 3 would not be linear in semilogarithmic scale. We can therefore conclude that we do not have very large amount of O_2^+ ions in our system. In Fig. 3 there are depicted two different data of the electron density. The rigorous evaluation procedure for gaining the electron density assuming general form of the EEDF is only the integration

of the EEDF. The electron density data based on the electron current at the plasma potential give only the idea about the error resulting from adopting the evaluation procedure based on the assumption of the Maxwellian EEDF. The error is actually not too great except for the later afterglow times. As one can infer from Fig. 4 there is a heating mechanism, which elevates the electron energy at later times after switching off the external source of power thus deforming the EEDF. In argon there are two metastable levels of excited atoms, namely $Ar(^3P_2)$ and $Ar(^3P_0)$. The spectroscopic measurements in an afterglow plasma under similar conditions have shown majority of $Ar(^3P_2)$ compared to $Ar(^3P_0)$ [12]. Most probably the heating is caused by mutual collisions of argon metastables, which results in an argon ion and electron with energy around 7.5 eV (Penning ionization). Such effect has been observed before in argon flowing afterglow [13]. It has been found in [13] that the density of argon metastables in the afterglow is roughly one order of magnitude greater than the electron density and thus the mutual collisions between argon metastables play important role in influencing the electron energy.

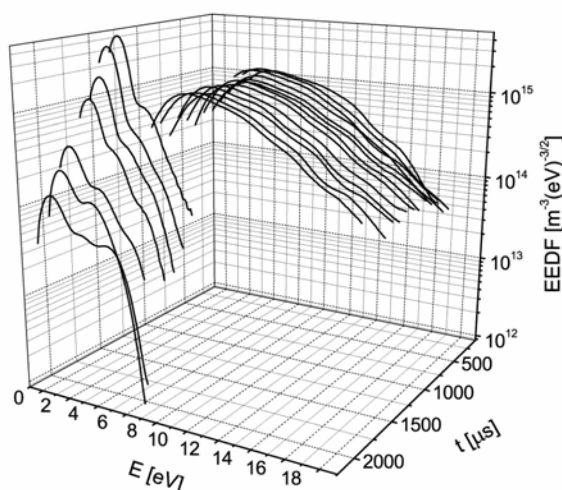

Fig. 5. Time evolution of the EEPF. The active part of the pulse starts at t = 0 s and ends at t = 775 µs.

The time dependence of the EEDF (normalized to electron density) is given in Fig. 5. The noise on the EEDF curves gives the idea about the accuracy of the data. It is clear from the figure that the EEDF in the active pulse does not have typical "double Maxwell" form, which has been calculated theoretically [14] as well as measured experimentally [15] in pure argon at low pressures. Instead, it has a Druyvesteyn-like form, which in comparison with Maxwellian EEDF lacks fast electrons. In the afterglow (idle) part of the modulation cycle the form of the EEDF changes drastically. Immediately noticeable is the substantial reduction of the effective temperature (much lower slope of the decreasing part of the EEDF) in comparison to that in the active pulse. Apparent is also excess of electrons with the energy around 2 eV ("hump" on the EEDF at that energy). This effect has not been observed when using pure argon as a working gas, and consequently it should be coupled with chemistry containing oxygen molecules. Possible mechanism may be that the electrons with energy around 7.5 eV, which originated from metastable-metastable collisions loose their energy in the dissociative attachment reaction forming the atomic O^- negative ions. This attachment reaction is energy-resonant [16] with the maximum for electron energies around 6 eV. That leaves for electrons that originated in such manner the energy around 1.5 eV. Note further, that the amplitude of the maxima of the EEDF in Fig. 5 decays approximately in linear manner in semilogarithmic scale. That supports conclusions of the discussion held above to the decay of electron density depicted in Fig. 3.

3.2 Application of the RF plasma jet for BSTO thin film deposition

In the single nozzle low-pressure plasma jet system it was possible to deposit $SrTiO_3$ and $Ba_xSr_{1-x}TiO_3$ thin films on Si and Pt surfaces. Maximum growth rate achieved was 250 – 300 nm/hour. Conditions used for deposition of BSTO films are given in Table 1.

***Table 1.** Experimental conditions for BSTO thin films depositions in single nozzle system.*

Sample no.	Q_{Ar} [sccm]	Q_{O2} [sccm]	P_{RF} [W]	Used nozzle	I_{RFm} [A]	U_{RFm} [V]
1	85	64	178	STO	3.6	259
2	85	64	219	STO,BTO	4.1	232
3	42	32	—	STO,BTO	—	—
4	42	13	180	STO,BTO	4.0	217
5	42	64	—	STO,BTO	—	—

Electron microprobe analysis has shown that chemical composition of deposited films is close to $SrTiO_3$ for sample no. 1. In BSTO layers $Ba_xSr_{1-x}TiO_3$ we have achieved $x \approx 0.56$ for samples nos. 2 and 3, $x \approx 0.47$ for sample no. 4 and $x \approx 0.44$ for sample no. 5. All the BSTO samples had Ti excess: Ti/(Ba+Sr) ≈ 22/17 and some oxygen excess. XRD patterns obtained from Bragg Brentano configuration for investigated samples can be seen in Fig. 6. Peaks belonging to $SrTiO_3$ perovskite phase and BSTO perovskite phase were identified. The BSTO peak is located between STO and BTO peaks of the standard depicted in the graph. It means that BSTO mixture contained approximately similar amount of Ba and Sr; in agreement with electron microprobe composition measurement. Small shift of BSTO peak close to STO peak of standard for samples nos. 4 and 5 shows that they should have Ba/Sr < 1. This fact also corresponds to the data from electron microprobe analysis.

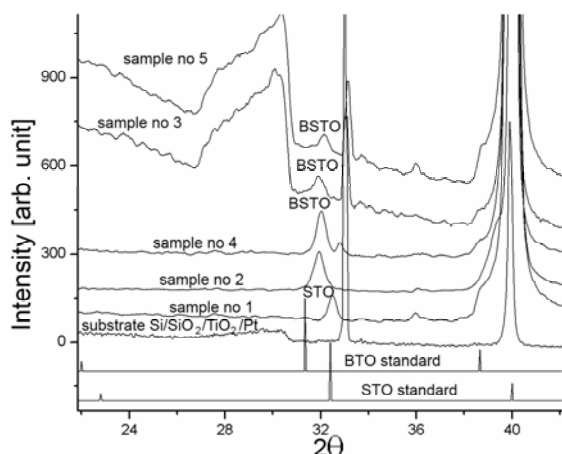

Fig. 6. X-ray diffraction patterns of deposited samples on Pt surface in Bragg Brentano geometry.

In order to perform more detailed study of crystalline structure, the sample no. 2 was analyzed by XRD in GI geometry (parallel beam). This method was more sensitive because for small angles between X-ray beam and the plane of the substrate surface the bigger volume of the film material is responsible for diffraction. Furthermore the influence of texture was less significant in this set up. Several diffraction peaks belonging to BSTO perovskite phase were also found. From the accurate position of detected BSTO diffraction peaks, it was possible to calculate lattice parameter $a = 3.980$ Å. Furthermore, it was possible to estimate the grain size of crystallites from the width of the diffraction peaks. The estimated grain size was 30 nm. This estimation is valid provided that we neglect the internal stresses in the films.

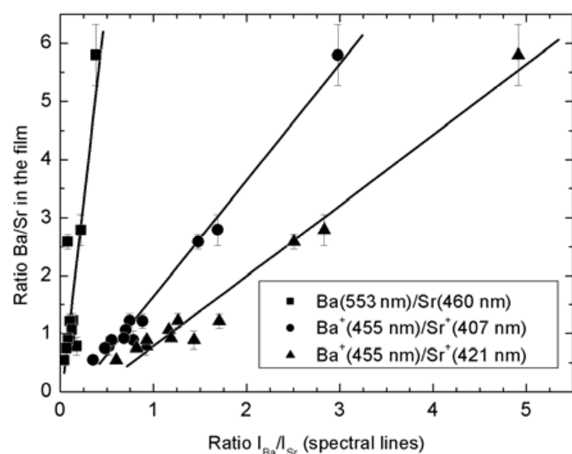

Fig. 7. The ratio of Ba and Sr contained in the film versus ratio of emission line intensities I_{Ba}/I_{Sr} and I_{Ba+}/I_{Sr+} measured close to substrate.

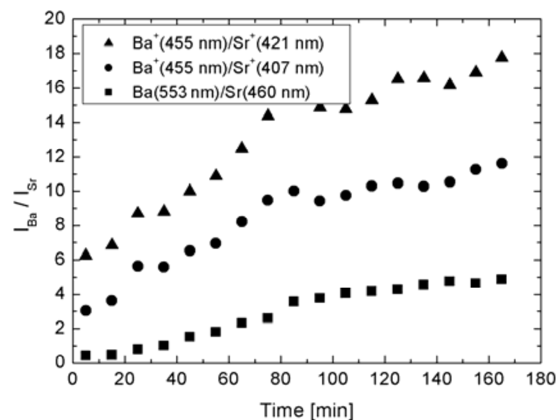

Fig. 8. Ratio of emission line intensities I_{Ba}/I_{Sr} and I_{Ba+}/I_{Sr+} during deposition of sample of compositional gradient BSTO film.

During deposition the plasma jet has been investigated by OES. In the spectra we have identified the lines of Sr and Ba sputtered excited atoms and of Ba^+ and Sr^+ ions. We already found out before [17] that the ratio of emission spectral line intensities of Ba and Sr atoms and of Ba^+ and Sr^+ ions is approximately proportional to the ratio of concentrations of the respective elements in the deposited film for the same geometry of the experimental setup, see Fig. 7. It means that the ratio of sputtered particles namely of Ba, Ba^+, Sr and Sr^+ from particular nozzles can be observed *in situ* by means of optical emission spectroscopy. That holds for the single nozzle system as well as for the double nozzle one. That in turn means that it is possible to control the stoichiometry of the deposited thin films by simply controlling the ratio of spectral line intensities during the process of deposition. This fact is very important and was used for deposition of compositional gradient BSTO films with increasing value of parameter x in stoichiometric formula $Ba_xSr_{1-x}TiO_3$ in dependence on the film thickness. In this experiment we fully exploited (i) the possibility of changing the average power by changing the duty cycle, i.e. the advantage of pulse operation and (ii) the possibility to change *independently* the average power to each nozzle, i.e. the advantage of the double nozzle system.

We intended to deposit the thin film with the ratio of Ba and Sr in the film increasing from the value 5:1 close to the substrate surface to the value 20:1 close to the thin film surface. Time evolution of the ratio of emission line intensities I_{Ba}/I_{Sr} and I_{Ba+}/I_{Sr+} during deposition of sample of compositional gradient BSTO film is given in Fig. 8. That ratio was controlled externally by changing the average power applied to respective nozzles. The power applied to both nozzles within the active pulse remained the same for whole deposition process. However, the *average* power for each nozzle was changed in a way that the increase of the duty cycle on the BTO nozzle was accompanied by the complementary decrease of the duty cycle on the STO nozzle. In our case we changed during the BSTO film deposition the duty cycle for BTO nozzle

from 160 μs /1.87 ms = 8.6 % up to 440 μs /1.87 ms = 23.5 % while keeping the repetition frequency constant and equal to that for STO nozzle, i.e. at 535 Hz. We expect that measurement of chemical composition of deposited films by means of electron microprobe will confirm presence of compositional gradient in the described sample of BSTO thin film.

Temperature of neutral particles is usually very close to the rotational temperature T_r in the discharge plasma. For measurement of this temperature we used 6 rotational lines of OH radicals (308 nm, Q_1 branch). Calculation of T_r was performed according equation

$$I_r = CA_j \sigma^4 \exp\left(\frac{-E_j}{kT_r}\right),$$

where C is constant that is the same for all lines in selected band, I_r is intensity of rotational line, A_j rotational transition probability, σ wave number, E_j excitation energy and k is the Boltzmann constant. Parameters needed for measurement of rotational temperature via Q_1 branch of OH are listed in the Table 2.

Table 2. Wavelengths, rotational quantum numbers of upper energetic level, intensity factors, excitation energies and rotational transition probabilities of selected lines from the Q_1 branch of OH rotational band ($A^2\Sigma^+ \rightarrow X^2\Pi_i$).

λ [nm]	J (Q_1)	i	E_j [cm^{-1}]	A_j
307.8440	3/2	0.563	32474.46	9.0
307.9951	5/2	1.065	32542.27	17.0
308.1541	7/2	1.582	32643.83	25.3
308.3278	9/2	2.100	32778.99	33.7
308.5196	11/2	2.640	32947.68	42.2
308.7338	13/2	3.160	33149.44	50.6

Using the above equation the rotational temperature can be calculated from the slope of a Boltzmann plot of ln ($I_r/(A_j\sigma^4)$) vs. Ej/k. Rotational temperature calculated for all deposited samples varied in the range 400 ÷ 500 K.

4. Conclusions

Low-pressure double hollow cathode plasma jet system was investigated during the $Ba_xSr_{1-x}TiO_3$ thin films deposition. Time resolved plasma parameters were determined by Langmuir probe measurement at the substrate position during the whole modulation cycle. Electron energy distribution was non-Maxwellian during the whole modulation cycle, with a strong deviation from Maxwellian in the afterglow plasma of the idle part of the cycle. Optical emission spectroscopy was used for measurement of rotational temperature of OH radicals and for controlled deposition of compositional gradient BSTO layers. It was shown that rotational temperature, which in discharge plasma is close to the temperature of neutral particles, is very low and varied in the range 400 ÷ 500 K.

Acknowledgments

The authors wish to acknowledge the financial support by the project 1QS100100563 of the Academy of Sciences of the Czech Republic. This work is a part of the research plan MSM 0021620834 that is financed by the Ministry of Education, Youth and Sports of the Czech Republic.

References

[1] L. Bárdoš, S. Berg, and H. Baránková. J. Vac. Sci. Technol. A **11**, 1486 (1993).
[2] L. Bárdoš and H. Baránková, Surf. Coat. Tech. **46**, 463 (2001).
[3] L. Soukup et al., Surf. Coat. Tech. **116-9**, 321 (1999).
[4] Z. Hubička, M. Šícha, L. Pajasová, L. Soukup, L. Jastrabík, D. Chvostová, and T. Wagner, Surf. Coat. Tech. **142**, 681 (2001).
[5] Z. Hubička, M. Čada, I. Jakubec, J. Bludská, Z. Málková, B. Trunda, P. Ptáček, J. Přidal, L. Jastrabík, Surf. Coat. Tech. **174**, 632 (2003).
[6] C.Y. Jin, Y. P. Ding, Z. Y. Meng, J. Inorg. Mater. **15**, 287 (2000).
[7] N. K. Pervez, P. J. Hansen, R. A. York, Appl. Phys. Lett. **85**, 4451 (2004).
[8] M. Čada, Z. Hubička, P. Adámek, P. Ptáček, H. Šíchová, M. Šícha, L. Jastrabík, Surf. Coat. Tech. **174**, 627 (2003).
[9] P. A. Chatterton, J. A. Rees, W. L. Wu, K. Al Assadi, Vacuum **42**, 489 (1991).
[10] M. J. Druyvesteyn. Z. Physik **64**, 781 (1930).
[11] S. Pfau, M. Tichý, Langmuir probe diagnostics of low-temperature plasmas, in Low Temperature Plasma Physics, R. Hippler et al. Eds., Wiley-VCH, Berlin etc., 2001, ISBN 3-527-28887-2, p. 131.
[12] O. Bockova, E.A. Sukisjan, Zhurnal prikladnoi spektroskopii **23** (1975) 601 (in Russian).
[13] J. Glosík, J. Pavlík, M. Šícha, M. Tichý, Czech. J. Phys. **B37**, 188 (1987).
[14] E. Passoth, J. F. Behnke, C. Csambal, M. Tichý, P. Kudrna, Y.B. Golubovskii, and I.A. Porokhova, J. Phys. D Appl. Phys. **32**, 2655 (1999).
[15] V. A. Godyak, R. B. Piejak, B. M. Alexandrovich, Plasma Sources Sci. Technol. **1**, 36 (1992).
[16] E. Stoffels, W.W. Stoffels, K. Tachibana, Rev. Sci. Instrum. **69** (1998) 117.
[17] J. Olejníček, Z. Hubička, P. Virostko, A. Deyneka, L. Jastrabík, D. Chvostová, H. Šíchová, J. Pokorný, Integrated Ferroelectrics **81**, 1 (2006).

*Corresponding author: hubicka@fzu.cz